Computerized Radiogrammetry of Third Metacarpal using Watershed and Active Appearance Model

Anu Shaju Areeckal, Mathew Sam, and Sumam David S., *Senior Member, IEEE*
Department of Electronics and Communication Engineering
National Institute of Technology Karnataka, Surathkal
Karnataka, India
anu_shaju_ec13f06@nitk.edu.in, pmathewsam@gmail.com, sumam@ieee.org

***Abstract*—Osteoporosis is a bone disorder, causing loss of bone mass and increased risk of fragility fracture. Osteoporosis can be diagnosed at a low cost using computerized metacarpal radiogrammetry of the third metacarpal bone of hand X-ray images. The most widely used methods for segmentation of hand bones are deformable models such as Active Shape Model (ASM), Active Appearance Model (AAM), etc. that make use of prior information of the shape and appearance of the object. However, due to the presence of other metacarpal bones having similar shape and size in its proximity, segmentation of third metacarpal bone in isolation becomes challenging and the deformable methods could fail. In this paper, we propose a method to automatically locate and segment the third metacarpal bone using marker-controlled watershed segmentation. Radiogrammetric measurements are determined automatically from the shaft of the third metacarpal bone and can be used to derive bone indices for the detection of bone loss due to osteoporosis. The measurements obtained from the proposed method and AAM are compared with ground truth. The results obtained show that the proposed approach is an efficient method for automated radiogrammetry of third metacarpal bone that can be used as a low cost tool for the early diagnosis of osteoporosis.**

***Index Terms*—Radiogrammetry, third metacarpal, AAM, watershed**

I. Introduction

Osteoporosis is a bone loss disorder, causing reduction in bone mass, degradation of bone micro-architecture and increased risk of fragility fracture. It is one of the major global concerns, causing a high morbidity and mortality especially in the elderly population. One of the emerging recent techniques in the diagnosis of osteoporosis is computerized metacarpal radiogrammetry, where cortical bone geometry is quantitatively assessed from one or more metacarpal bones [1], [2]. Cortical bone indices calculated from the radiogrammetric measurements are used to measure bone loss due to osteoporosis. Since radiogrammetric measurement of a single metacarpal bone is sufficient to measure the bone loss and the third metacarpal bone can be identified easily irrespective of the hand orientation, we choose the third metacarpal as our object of interest.

One of the most widely used methods for segmentation of hand bones is the use of deformable models, that make use of prior shape and feature information available from the object-of-interest. Deformable models such as Active Shape Model (ASM) make use of a prior shape model of the object, while Active Appearance Model (AAM) combines shape and texture information [3]. ASM and AAM have been used for various applications, such as bone densitometry, diagnosis of rheumatoid arthritis, bone age assessment, etc. The advantages of deformable models are high accuracy and robustness to image contrast and noise, and hence makes it a reliable method for images with different acquisition conditions. However, there are concerns regarding use of AAM for segmentation of third metacarpal bone alone. The presence of other metacarpal and phalanx bones, that have similar shape and appearance, lying in the proximity of the third metacarpal bone poses a great challenge to the segmentation of third metacarpal using deformable models. The accuracy of AAM depends on the images used for the training set, which requires manual annotations that is very time consuming.

The objective of this paper is to propose a simple and efficient approach to automatically locate and segment the third metacarpal bone and to measure the radiogrammetric measurements automatically from the bone shaft.

Watershed segmentation is a hybrid region growing technique that creates watershed lines across the object boundary. The advantage of watershed segmentation is its simplicity and ease of use. It works well for images with good contrast between the bone edge and background. A drawback of watershed is its sensitivity to the gradient image used and over-segmentation due to presence of local minima. The former problem can be alleviated by proper preprocessing techniques to remove noise and improve the contrast of image. The latter problem can be prevented by the use of markers in the image to level out the local minima.

The remaining paper is organized as follows: Section 2 describes the proposed methodology, section 3 discusses the implementation of AAM, section 4 compares the performance of watershed and AAM segmentation methods and section 5 concludes the work.

II. Proposed Methodology

The proposed approach use intensity profile, mathematical morphology and watershed segmentation for automatic detection and delineation of the third metacarpal bone. Figure 1 shows a flowchart of the proposed approach. This approach is a modified version of our previous method [4].

978-1-5090-5949-2/18/$31.00 ©2018 IEEE

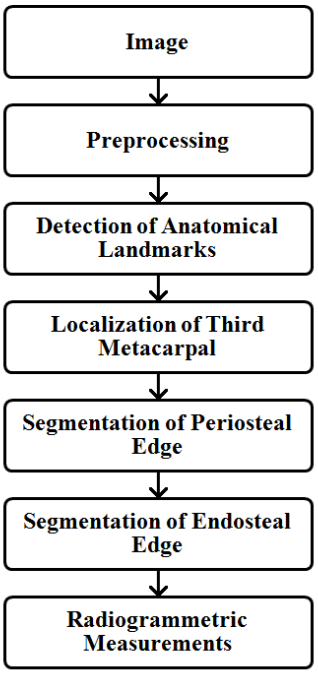

Fig. 1: Flowchart of the proposed methodology

A. Preprocessing

Preprocessing of hand images before segmentation is essential to improve the accuracy of segmentation. Due to different image acquisition conditions, contrast of images may vary. Contrast of the hand X-ray image is enhanced by linearly mapping the pixel values to the full dynamic range. The image is then denoised using Block Matching 3D (BM3D) method [5]. BM3D is an edge preserving technique which effectively removes noise from hand image without blurring the bone edges. In order to increase the contrast between bones and surrounding soft tissue, a soft tissue subtraction is employed using a large Gaussian filter with standard deviation of 200 pixels. This results in a hand bone image, containing bone region alone.

B. Detection of anatomical landmarks

The third metacarpal bone is automatically detected from the hand bone image with the help of two anatomical landmarks, (1) the tip of third distal phalanx (TDP), and (2) the Distal Radius-Ulnar Joint (DRUJ). To find the anatomical landmarks automatically, the hand region is extracted by thresholding the denoised image using Otsu's method and finding the largest connected component [6]. Bounding box of the hand is determined and its upper border will contain anatomical landmark, TDP.

The second anatomical landmark is determined as follows. The binary image of the soft tissue subtracted image is found by a combination of global and local thresholding. Otsu's thresholding of the soft tissue subtracted image may fuse closely spaced bones in the binary image. Niblack's local thresholding method gives a good binary image of the hand bone region, but also results in noisy white patches in the background [7]. Hence, the intersection of resultant images of the Otsu's and Niblack's methods is used as the binary image of hand bone region. DRUJ is found by observing the intensity profiles at intervals of five rows, starting from the lower border of the binary image. The row containing DRUJ will have a single peak, while the rows below DRUJ show two distinct peaks, as shown in figure 2.

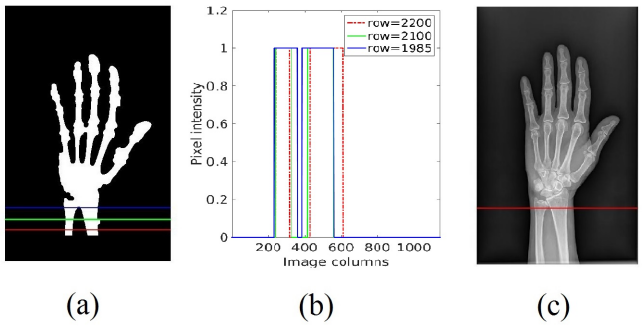

Fig. 2: Detection of the anatomical landmark at distal radius-ulnar junction (DRUJ): (a) and (b) Intensity profiles along different rows at the lower half of the binary image, and (c) detection of the row containing DRUJ point

C. Localization of third metacarpal bone

From the two anatomical landmarks, the row corresponding to the third metacarpal centroid is estimated to be at an average distance of 125 mm below TDP and 70 mm above DRUJ. These distance measures were found empirically by observing the images in the dataset. An intensity profile along the row containing the centroid of the third metacarpal bone in the soft tissue subtracted image is plotted. The prominent peaks of the noisy intensity profile obtained is filtered using a zero-phase digital filter, as shown in figure 3. The third most prominent peak is taken as the centroid of the third metacarpal bone.

The third metacarpal bone should be vertically aligned for accurate segmentation results. To find the angle of orientation

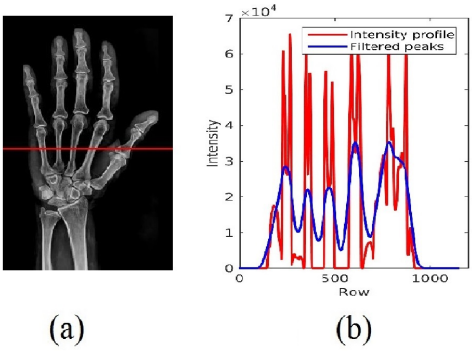

Fig. 3: Detection of third metacarpal centroid: (a) Row containing the centroid estimated from anatomical landmarks and (b) Corresponding intensity profile and filtered peaks

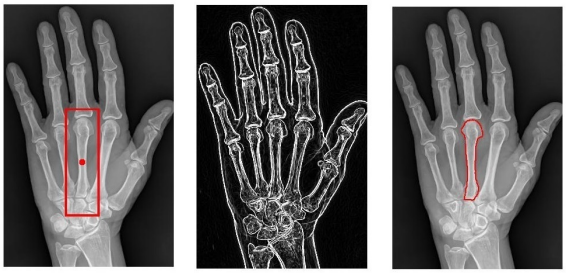

Fig. 4: Segmentation of periosteal edge: (a) Internal and external markers, (b) gradient image, and (c) segmented third metacarpal bone

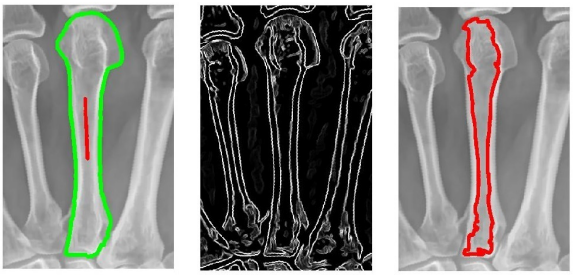

Fig. 5: Segmentation of endosteal edge: (a) Internal and external markers, (b) gradient image for the watershed segmentation, and (c) segmented endosteal edge

of the third metacarpal bone, the third most prominent peaks of two intensity profiles along rows 5 mm above and below the third metacarpal centroid is interpolated and the central axis of the third metacarpal is determined. The hand image is rotated by the angle of orientation. The vertically aligned image is then used for watershed segmentation.

D. Segmentation using Watershed

In order to prevent oversegmentation, marker-controlled watershed is employed. Centroid of the third metacarpal bone, morphologically dilated by a disk structuring element of size 2 mm, is used as the inner marker for periosteal edge segmentation. External marker used is a rectangular box with borders 45 mm above and below the centroid and 14 mm on either sides of the centroid. To overcome the leakage of watershed lines at bone edge discontinuities, a morphological viscous closing of the gradient image is done. Applying marker-controlled watershed segmentation on the gradient image will create segmentation lines along the boundary of the third metacarpal bone, as shown in figure 4.

Radiogrammetry is done on the shaft of the third metacarpal bone, which is our Region-of-Interest (ROI). ROI is automatically extracted by discarding 35% of the upper and lower regions of the segmented third metacarpal bone. In order to detect the inner edge of the cortical bone, watershed is again applied. The segmented outer edge of the third metacarpal bone is used as the external marker. The medial line of the bone shaft ROI acts as the inner marker. In order to further enhance the contrast of the cortical bone and inner bone shaft, the segmented third metacarpal bone is filtered using Gaussian filter with standard deviation of 10 pixels and the morphological gradient image is determined. Using this image as the segmentation function and the external and internal markers, watershed segmentation is applied to delineate the inner edge of the third metacarpal bone, as shown in figure 5.

E. Metacarpal radiogrammetry

Radiogrammetric measurements are taken from the automatically detected bone shaft of the third metacarpal bone, as shown in figure 6. Cortical width (CW) is measured by averaging the total number of pixels in the segmented ROI. Medullary width (MW) is measured by averaging the total number of pixels in the segmented inner bone shaft region. Many bone indices have been formulated from the radiogrammetric measurements for the detection of bone loss in osteoporosis. Combined Cortical Thickness (CCT) is a simple bone index that measures the cortical bone thickness along the bone shaft by calculating the difference between CW and MW.

III. Active Appearance Model

Active Appearance Model (AAM) is a popular method used for segmentation of hand bones. AAM is modeled with a set of training images with manually annotated landmarks. Each training image is landmarked along the edges of the object to be segmented at the same positions with respect to the object in each image. AAM forms a mean shape and appearance model with these landmarks, by first aligning the shapes by translation, scaling and rotation and then using Principal Component Analysis (PCA) to describe the variation of the aligned shapes among individuals. Information about the relative position of these points are also acquired in the form of line profile, where the normal distance between a line joining adjacent landmarks and a contour edge is also recorded. The mean shape is stored along with possible variations of the shape and appearance of the object. A new image can be segmented by finding the best match of the model to the image data.

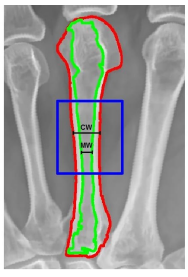

Fig. 6: Third metacarpal bone shaft used for radiogrammetric measurements

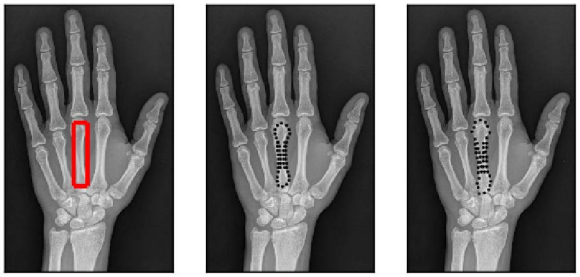

Fig. 7: Testing the trained AAM model: (a) Initial bounding box detection, (b) Initial position of the AAM model and (c) Final segmented third metacarpal bone

A. Creating the AAM model

To build the AAM model, the dataset is divided into a training set and a test set. A template with 46 landmark points is used to manually annotate the third metacarpal bone in the training set [8]. Twenty eight points are used to demark the outer and inner edges of the bone shaft. The annotated training images are cropped to the bounding box of the landmark points with 20% padding around the boundary. The cropped images are rescaled if the image diagonal has more than 400 pixels. The landmark points in the training set are stored as bounding boxes using DLib detector. AAM model and its shape and appearance variations are generated using holistic AAM approach with Fast Dense Scale Invariant Feature Transform (DSIFT) features, 20 shape components and 150 appearance components.

B. Fitting the AAM model

Once the AAM is built, it can be used for the segmentation of third metacarpal bone in new test images. The test image is first vertically aligned with respect to the third metacarpal bone, in order to prevent misdetection of the third metacarpal. The AAM model can then be fitted into the rotated test images. The fitting of the model on a test image is done in an iterative process. The bounding box of the third metacarpal bone is detected using the DLib detector. The center of gravity of the model is aligned with the center of gravity of the test image. The location of the landmarks are iteratively changed to minimize the distance between the acquired landmarks from fitting the model and the edge of the metacarpal being segmented. The AAM model is fitted using Lucas Kanade optimization, as shown in figure 7. The fitted landmark locations are extracted and interpolated to determine the cortical thickness along the metacarpal bone shaft.

IV. Results and Discussion

A. Data used

A dataset of 138 hand X-ray images (Postero-Anterior view) of healthy and osteoporotic people were collected from two hospitals in India. Data included men and women above the age of 30 years. The images were acquired using 400mA Allengers HF Advantage (deviation index of -2.25 to 3.6) and DR Agfa DX-D 300 (X-ray tube voltage=52kV, X-ray tube current=160mA, exposure time=32ms, source-to-object distance of 990 to 1370mm and deviation index of -8.1 to -1.8). DXA scans of lumbar spine of the patients were used to categorize them into healthy (T-score ≥ -1) and low bone mass groups (T-score < -1).

B. Comparison of performance with manual segmentation

The proposed method was implemented using Matlab R2015a and SDC toolbox for Matlab [9]. AAM was implemented using Menpo package in Python [10].

A total of 39 training images with 46 manually annotated landmarks were used to create the AAM model. AAM was able to correctly identify and segment the third metacarpal bone in 81% of the images. Whereas, the proposed approach was able to accurately detect the third metacarpal centroid in 94% of the images, and correctly segment the third metacarpal bone edges in 89% of the dataset.

Manual segmentation of five images at the third metacarpal bone shaft ROI are used to evaluate the segmentation results of the proposed and AAM methods. Figure 8 shows the manual segmentation, proposed segmentation and AAM results of a healthy subject (1a-1c), subject with low bone mass (2a-2c) and subject with osteoporosis (3a-3c). Automated segmentation results are quantitatively evaluated using the following performance metrics.

Jaccard Measure (JM) is a measure of the overlap between segmented regions of manual ($Area_{man}$) and automated ($Area_{auto}$) segmentation methods. Percent Area Difference (PAD) is the percentage of differences in area of the manual and automated segmentation techniques.

$$JM = \frac{|Area_{auto} \cap Area_{man}|}{|Area_{auto} \cup Area_{man}|} \tag{1}$$

$$PAD = \frac{|Area_{auto} - Area_{man}|}{Area_{man}} \tag{2}$$

Pixel-wise comparison of the segmentation results is done using confusion matrix. A cortical bone pixel in the ROI being correctly segmented as cortical bone is taken as true positive case (TP), and the background and soft tissue pixels being segmented as background is the true negative case (TN). The case when a cortical bone pixel is misclassified as background and a background pixel is misclassified as cortical bone are the False Negative (FN) and False Positive (FP) cases, respectively. Evaluation metrics derived from the confusion matrix are recall, precision and F1 score. Recall is the sensitivity of detection of positive pixels. Precision is the fraction of true positive pixels among all pixels detected as positive. F1 score measures the segmentation accuracy and is calculated as the harmonic mean of recall and precision, as shown below.

$$Recall = \frac{TP}{TP + FN} \tag{3}$$

$$Precision = \frac{TP}{TP + FP} \tag{4}$$

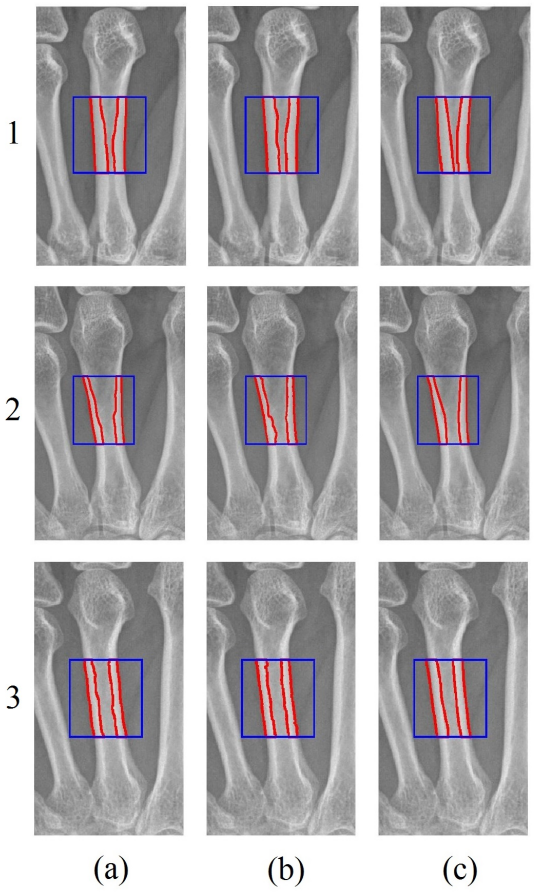

Fig. 8: Segmentation results of healthy (image 1), low bone mass (image 2) and osteoporotic subjects (image 3): (a) Manual segmentation, (b) proposed segmentation method and (c) segmentation using AAM

$$F1\ score = 2 \times \frac{Recall \times Precision}{Recall + Precision} \tag{5}$$

Table I shows the performance evaluation of proposed method and AAM with manual segmentation. The proposed method shows a higher mean Jaccard Measure (JM=0.9) and lower mean percent area difference (PAD=0.03) than the AAM method (JM=0.82 and PAD=0.11). Average recall measure is comparable in both the methods. Average precision and F1 score are higher for the proposed method (precision=0.94, F1 score=0.95) as compared to AAM (precision=0.86, F1 score=0.90).

C. Validation with ground truth measurements

Ground truth cortical measurements of hand X-ray images belonging to 6 healthy and 8 people with low bone mass were obtained from experts. The radiogrammetric measurements obtained at the third metacarpal bone mid-shaft using both the proposed and AAM methods are compared to ground truth measurements of 14 images. Table II reports the absolute error obtained in measurement of cortical width and medullary width in each of the 14 cases.

Comparison of CW measurements show a mean absolute error of 0.04 mm (0.51%) and 0.12 mm (1.54%) for the proposed method in the healthy and low bone mass groups, respectively. AAM segmentation shows mean absolute error of 0.43 mm (4.78%) and 0.43 mm (5.08%) in the healthy and low bone mass groups, respectively. In the case of MW measurements, the proposed method gives a mean absolute error of 0.22 mm (5.81%) in the healthy group and 0.26 mm (7.86%) in the low bone mass group. Whereas AAM method shows an absolute error of 0.12 mm (3.66%) in the healthy group and 0.37 mm (11.10%) in the low bone mass group. CCT of the third metacarpal midshaft obtained from the proposed method show 0.2 mm mean absolute error (4.26%) in the healthy group and 0.17 mm mean absolute error (4.18%) in the low bone mass group. CCT measurements of the AAM method show mean absolute error of 0.47 mm (9.68%) in the healthy group and mean absolute error of 0.54 mm (11.40%) in the low bone mass group. This shows that the proposed segmentation approach is a simple and efficient method that can be used to measure radiogrammetric parameters for the calculation of bone indices.

The proposed method has certain limitations. Even though the proposed method was able to detect the third metacarpal centroid in 94% of the images, the segmentation of edges at the bone shaft was poor for 11% of the images. This is mainly due to different acquisition conditions of the images in the dataset. Although AAM has the advantage of being robust to image contrast, the accuracy depends heavily on the number and type of images used in the training set. In this work, cortical bone is delineated using 28 points along the metacarpal bone shaft, using the 46-landmark template. To improve accuracy of CCT measurement, a template with larger number of landmarks must be used, which is a hideous task. Moreover, in this specific application, AAM can easily misdetect the third metacarpal. Hence, the work presented in this paper proposes a simple technique to automatically detect and segment the third metacarpal bone shaft for radiogrammetric measurements.

V. Conclusion

A simple and fully automated approach for segmentation of third metacarpal bone and extraction of radiogrammetric measurements from hand X-ray images has been proposed. The proposed method uses intensity profiles and marker-controlled watershed segmentation for automatic detection and delineation of the outer and inner bone edges of the metacarpal bone shaft. A dataset of 138 healthy and osteoporotic people from India were used. The proposed method was compared with segmentation using AAM model built from the same dataset. The proposed method was able to automatically locate and correctly segment the third metacarpal bone in 89% images, while AAM detected third metacarpal in 81% images. Quantitative evaluation of the automated methods with manual segmentation results showed better performance values for the proposed method as compared to AAM. Comparison of the proposed method with ground truth CCT measurements showed a mean absolute error of 0.2 mm and 0.17 mm in

TABLE I: Performance evaluation with manual segmentation

Images	Jaccard Measure		Percent Area Difference		Recall		Precision		F1 score	
	Proposed	AAM	Proposed	AAM	Proposed	AAM	Proposed	AAM	Proposed	AAM
1	0.91	0.84	0.01	0.01	0.96	0.91	0.95	0.91	0.95	0.91
2	0.94	0.82	0.02	0.03	0.96	0.92	0.98	0.89	0.97	0.90
3	0.88	0.84	0.10	0.16	0.99	0.99	0.90	0.85	0.94	0.91
4	0.87	0.76	0.03	0.15	0.94	0.93	0.92	0.81	0.93	0.86
5	0.90	0.83	0.01	0.18	0.95	0.99	0.94	0.84	0.95	0.91
Mean	**0.90**	**0.82**	**0.03**	**0.11**	**0.96**	**0.95**	**0.94**	**0.86**	**0.95**	**0.90**

TABLE II: Comparison of radiogrammetric measurements with ground truth

	Images	Ground truth		Proposed method				AAM segmentation			
		Actual CW (mm)	Actual MW (mm)	Measured CW (mm)	Absolute error (mm)	Measured MW (mm)	Absolute error (mm)	Measured CW (mm)	Absolute error (mm)	Measured MW (mm)	Absolute error (mm)
Healthy	1	8.75	4.19	8.72	0.03	3.54	0.65	8.33	0.42	4.18	0.01
	2	9.14	4.42	9.04	0.10	4.17	0.25	8.69	0.45	4.58	0.16
	3	10.45	5.85	10.43	0.02	5.84	0.01	9.74	0.71	5.68	0.17
	4	8.89	3.98	8.90	0.01	3.75	0.23	8.56	0.33	3.92	0.06
	5	7.55	2.62	7.51	0.04	2.57	0.05	7.10	0.45	2.79	0.17
	6	7.72	2.22	7.78	0.06	2.09	0.13	7.53	0.19	2.38	0.16
	Mean				**0.04**		**0.22**		**0.43**		**0.12**
Low bone mass	7	6.61	2.89	6.39	0.22	2.36	0.53	6.86	0.25	3.14	0.25
	8	10.27	4.92	9.96	0.31	4.45	0.47	8.94	1.33	4.97	0.05
	9	7.94	2.63	7.98	0.04	2.73	0.10	8.00	0.06	3.09	0.46
	10	7.89	3.18	7.92	0.03	3.27	0.09	7.97	0.08	4.21	1.03
	11	8.48	4.20	8.34	0.14	4.14	0.06	7.99	0.49	4.68	0.48
	12	8.44	2.92	8.40	0.04	3.06	0.14	8.16	0.28	2.96	0.04
	13	6.73	3.17	6.53	0.20	2.50	0.67	7.34	0.61	3.51	0.34
	14	8.48	4.88	8.48	0.00	4.93	0.05	8.82	0.34	5.16	0.28
	Mean				**0.12**		**0.26**		**0.43**		**0.37**

the healthy and low bone mass groups, respectively. Whereas AAM showed a mean absolute error of 0.47 mm and 0.54 mm in the healthy and low bone mass groups, respectively. The proposed segmentation technique was found to outperform AAM and hence could be used efficiently for diagnosis of osteoporosis using third metacarpal radiogrammetry.

ACKNOWLEDGMENT

We would like to thank TEQIP-II Office, National Institute of Technology Karnataka, Surathkal, India, for supporting data collection, and the Institutional Ethics Committee, Kasturba Medical College Hospital, Mangalore, Manipal Academy of Higher Education, India, for approving the study protocol. We would like to thank the Department of Orthopedics, District Wenlock Hospital, Mangalore, India and Tejaswini Hospital, Mangalore, India, for their help in this study.

REFERENCES

[1] A. Rosholm, L. Hyldstrup, L. Baeksgaard, M. Grunkin, and H. Thodberg, "Estimation of bone mineral density by digital X-ray radiogrammetry: Theoretical background and clinical testing," *Osteoporosis Int.*, vol. 12, no. 11, pp. 961–969, 2001.

[2] H. Thodberg, R. Van Rijn, T. Tanaka, D. Martin, and S. Kreiborg, "A paediatric bone index derived by automated radiogrammetry," *Osteoporosis Int.*, vol. 21, no. 8, pp. 1391–1400, 2010.

[3] T. F. Cootes, G. J. Edwards, and C. J. Taylor, "Active appearance models," *IEEE Trans. Pattern Anal. and Mach. Intell.*, no. 6, pp. 681–685, 2001.

[4] A. S. Areeckal, S. S. David, M. Kocher, N. Jayasheelan, and J. Kamath, "Fully automated radiogrammetric measurement of third metacarpal bone from hand radiograph," in *Proc. 2016 Int. Conf. Signal Process. and Commun. (SPCOM)*. IEEE, 2016, pp. 1–5.

[5] K. Dabov, A. Foi, V. Katkovnik, and K. Egiazarian, "Image denoising by sparse 3-D transform-domain collaborative filtering," *IEEE Trans. Image Process.*, vol. 16, no. 8, pp. 2080–2095, 2007.

[6] N. Otsu, "A threshold selection method from gray-level histograms," *Automatica*, vol. 11, no. 285-296, pp. 23–27, 1975.

[7] N. Wayne, *An Introduction to Digital Image Processing*. Prentice Hall, Eaglewood Cliffs, New Jersey, 1986.

[8] M. Sam, A. S. Areeckal, and S. David S, "Early diagnosis of osteoporosis using active appearance model and metacarpal radiogrammetry," in *Proc. 13th Int. Conf. Signal-Image Technol. and Internet-Based Syst. (SITIS)*. IEEE, 2017, pp. 173–178.

[9] E. R. Dougherty, R. A. Lotufo, and T. I. S. for Optical Engineering SPIE, *Hands-on Morphological Image Processing*. SPIE Optical Engineering Press Washington, 2003, vol. 71.

[10] The Menpo Project- http://www.menpo.org.